Stem Cell Reports
Article
ISSCR
OPEN ACCESS

Patient-Specific iPSC Model of a Genetic Vascular Dementia Syndrome Reveals Failure of Mural Cells to Stabilize Capillary Structures

Joseph Kelleher,[1,2,3] Adam Dickinson,[1,2] Stuart Cain,[1,4] Yanhua Hu,[5] Nicola Bates,[1,4] Adam Harvey,[6] Jianzhen Ren,[1,2,3] Wenjun Zhang,[1,2,3] Fiona C. Moreton,[7] Keith W. Muir,[7] Christopher Ward,[1] Rhian M. Touyz,[6] Pankaj Sharma,[8] Qingbo Xu,[5] Susan J. Kimber,[1,4,*] and Tao Wang[1,2,3,*]

[1]School of Biological Sciences, Faculty of Biology, Medicine and Health, The University of Manchester, Manchester, UK
[2]Manchester Centre for Genomic Medicine, Manchester University NHS Foundation Trust, Manchester, UK
[3]Division of Evolution and Genomic Sciences, The University of Manchester, Manchester, UK
[4]Division of Cell Matrix Biology and Regenerative Medicine, The University of Manchester, Manchester, UK
[5]Cardiovascular Division, BHF Centre, King's College London, London, UK
[6]Institute of Cardiovascular & Medical Sciences, University of Glasgow, Glasgow, UK
[7]Institute of Neuroscience and Psychology, University of Glasgow, Glasgow, UK
[8]Institute of Cardiovascular Research Royal Holloway University of London (ICR2UL), London, UK
*Correspondence: tao.wang@manchester.ac.uk (T.W.), sue.kimber@manchester.ac.uk (S.J.K.)
https://doi.org/10.1016/j.stemcr.2019.10.004

SUMMARY

CADASIL (cerebral autosomal dominant arteriopathy with subcortical infarcts and leukoencephalopathy) is the most common form of genetic stroke and vascular dementia syndrome resulting from mutations in *NOTCH3*. To elucidate molecular mechanisms of the condition and identify drug targets, we established a patient-specific induced pluripotent stem cell (iPSC) model and demonstrated for the first time a failure of the patient iPSC-derived vascular mural cells (iPSC-MCs) in engaging and stabilizing endothelial capillary structures. The patient iPSC-MCs had reduced platelet-derived growth factor receptor β, decreased secretion of the angiogenic factor vascular endothelial growth factor (VEGF), were highly susceptible to apoptotic insults, and could induce apoptosis of adjacent endothelial cells. Supplementation of VEGF significantly rescued the capillary destabilization. Small interfering RNA knockdown of *NOTCH3* in iPSC-MCs revealed a gain-of-function mechanism for the mutant *NOTCH3*. These disease mechanisms likely delay brain repair after stroke in CADASIL, contributing to the brain hypoperfusion and dementia in this condition, and will help to identify potential drug targets.

INTRODUCTION

CADASIL (cerebral autosomal dominant arteriopathy with subcortical infarcts and leukoencephalopathy), a systemic small vessel disease (Joutel et al., 1996, 1997; Sharma et al., 2001; Wang et al., 2008), is the most common type of genetic stroke syndrome and vascular dementia. Although clinical presentations are diverse (Bentley et al., 2011) and disease severity varies among patients, the underlying pathologies are unique in small arteries, including degeneration of vascular smooth muscle cells (VSMCs), accumulation of NOTCH3 extracellular domain proteins (N3ECD), and deposition of granular osmiophilic material (Joutel et al., 2000). Valuable insights into disease pathologies have been uncovered using animal or cell models (Joutel et al., 2000); however, the molecular mechanisms underpinning the condition are still largely unknown, and thus no effective treatment is available. The majority of the CADASIL *NOTCH3* mutations do not disrupt canonical NOTCH3 signaling (Monet et al., 2007), and Notch3$^{-/-}$ mice do not develop the CADASIL phenotype (Domenga et al., 2004); therefore, this condition does not seem to be caused by a simple loss of NOTCH3 function.

Notch proteins are single-pass transmembrane receptors mediating an evolutionarily conserved signaling pathway (Artavanis-Tsakonas et al., 1999). Ligand binding triggers sequential Notch protein cleavages that release the intracellular domain (NICD). The NICD then translocates into the nucleus, where it activates the canonical Notch signaling pathway, regulating the expression of Notch target genes including hairy and enhancer of split (*HES*) and Hairy-related transcription factor (*HRT/HEY*). *NOTCH3* is specifically expressed in the arterial smooth muscle cells (SMCs) and pericytes, collectively called mural cells (MCs), and supports VSMC differentiation and MC survival (Joutel, 2011; Wang et al., 2012, 2014). However, a full picture of NOTCH3 function in MCs is still unclear.

In addition to VSMC pathology, abnormal endothelial cells (ECs) and impaired shear stress-induced or endothelium-dependent vasodilatation were also observed in small arteries of CADASIL patients (Dubroca et al., 2005; Stenborg et al., 2007). *NOTCH3* expression is usually very low or absent in ECs, which brings into question the primary involvement of ECs in CADASIL pathology. In intact arteries, a positive feedback loop exists between the Notch ligand Jagged1 in ECs and NOTCH3 in the adjacent VSMCs, which is fundamental for both arterial development and the functional maintenance of mature arteries (Liu et al., 2009, 2010). The EC-MC communication via Notch signaling is likely perturbed by the *NOTCH3* mutation in CADASIL. However, this has never been demonstrated experimentally. Recent data revealed a substantial

reduction of capillary density in the white matter of CADASIL mice resulting in hypoperfusion in the brain (Joutel et al., 2010), which suggests an angiogenesis-related failure. Pericytes, the perivascular cells surrounding capillaries, play a key role in the process of angiogenesis, supporting capillary stability and EC survival (Sweeney et al., 2016). Interestingly, the NOTCH3 signaling pathway has recently been identified to be crucial in regulating pericyte number and for proper angiogenesis and MC investment (Liu et al., 2010; Wang et al., 2014). However, to our knowledge, the impact of *NOTCH3* mutation on angiogenesis in CADASIL has never been investigated previously.

To date, up to ten transgenic CADASIL mouse models have been generated. Although recent models appear much improved (Joutel, 2011; Wallays et al., 2011), the CADASIL mice did not phenocopy the full spectrum of clinical features seen in CADASIL patients, especially the brain pathologies. Previous cell-based CADASIL studies have mainly used overexpression of mutant NOTCH3 in non-vascular cell lines (Bentley et al., 2011; Joutel et al., 2004; Peters et al., 2004). Given the fact that the Notch signaling is highly dosage and context dependent, the strategy of overexpression may not faithfully reflect the true pathological defects in the vascular cells of CADASIL patients.

It is now possible to generate patient-specific disease models without overexpressing mutant gene products. By co-transfecting key pluripotency-associated factors (*OCT3/4*, *SOX2*, *C-MYC*, and *KLF4*), adult somatic cells can be reprogrammed to induced pluripotent stem cells (iPSCs) that have potential to differentiate into cells from all three embryonic germ layers (Takahashi and Yamanaka, 2006). iPSC-derived cells carry the genetic information of the donor and therefore represent patient-specific disease models to be used for elucidating disease mechanisms and for *in vitro* high-throughput drug screening (Tiscornia et al., 2011).

In this study, we have successfully established iPSCs from CADASIL patients. The iPSCs were differentiated into ECs and MCs. Phenotypic characterization of the iPSC disease model identified failure of the iPSC-derived MCs (iPSC-MCs) to stabilize angiogenic capillary structures and support iPSC-derived EC (iPSC-EC) survival, suggesting a defect of pericyte function. The CADASIL iPSC-MCs had downregulation of *PDGFRβ* (*platelet-derived growth factor receptor β*) and reduced secretion of vascular endothelial growth factor (VEGF). Supplement of VEGF or small interfering RNA (siRNA) knockdown of *NOTCH3* significantly rescued the phenotypes. Key findings obtained from the iPSC model were also confirmed on primary VSMCs isolated from CADASIL patients. The novel molecular mechanisms uncovered by using the new patient-specific iPSC model could advance our knowledge of this genetic condition and vascular dementia in general, and contribute to the future development of novel therapies.

RESULTS

Generation of Disease-Specific iPSC Lines

Human dermal fibroblasts (HDFs) were obtained from skin biopsies of two CADASIL patients carrying the mutations Arg153Cys and Cys224Tyr (Figures S1A and S1B), respectively, and two control individuals (Figures S1C and S1D). One of the control individuals was an unaffected sibling of the patient who carries the Cys224Tyr mutation. The HDFs were transformed into iPSCs by Sendai virus (SeV) delivery of transcription factors *OCT4*, *SOX2*, *KLF4*, and *C-MYC* (Figure S2A). Twenty-eight days after virus infection, multiple colonies (12–18 clones from each line) were selected and expanded, and the expression of the pluripotency-associated genes, *OCT4*, *SOX2*, and *NANOG*, was confirmed in the iPSCs (Figure S2B). A subset of clones was karyotyped (Figure S2C) and screened for residual SeV carried over from the initial infection. All selected clones were free of SeV after ten passages (Figure S2D). The reprogrammed cells were able to form embryoid bodies, which expressed ectoderm, mesoderm, and endoderm marker genes (Figure S2E), confirming the pluripotency of the cells. Thus, we established two patient-specific iPSC lines and two control iPSC lines. Based on the characterization described above, three clones from each iPSC line with normal karyotypes were randomly chosen for the subsequent work.

Differentiation of iPSCs into ECs and MCs

ECs and MCs, the two major vascular cell types, were differentiated from the healthy and CADASIL iPSCs. For EC differentiation, iPSCs were treated with a combination of growth factors for 12 days as shown schematically in Figure 1A. On day 3, monolayers of broader cells with a cobblestone appearance started to emerge from the edges of the tightly packed colonies. After bone morphogenetic protein (BMP) withdrawal and addition of VEGF on day 6 to promote EC differentiation, the cobblestone-like cells expanded and persisted through the course of differentiation (Figure 1B). Over the 12-day differentiation period, the expression of pluripotency-associated genes (*OCT4*, *SOX-2*, and *NANOG*) decreased progressively (Figure 1C). On day 3 after increased dosage of BMP4, a transient expression of the *T* gene was observed, indicating early mesoderm commitment. This was followed by an increase in additional mesoderm markers, *ISL1* and *MESP1*, which peaked on day 6. After addition of VEGF on day 6, the endothelial specific markers, *VE-CADHERIN* and *PECAM-1/CD31*, as well as *KDR*, were significantly induced and reached a plateau by day 12 of differentiation.

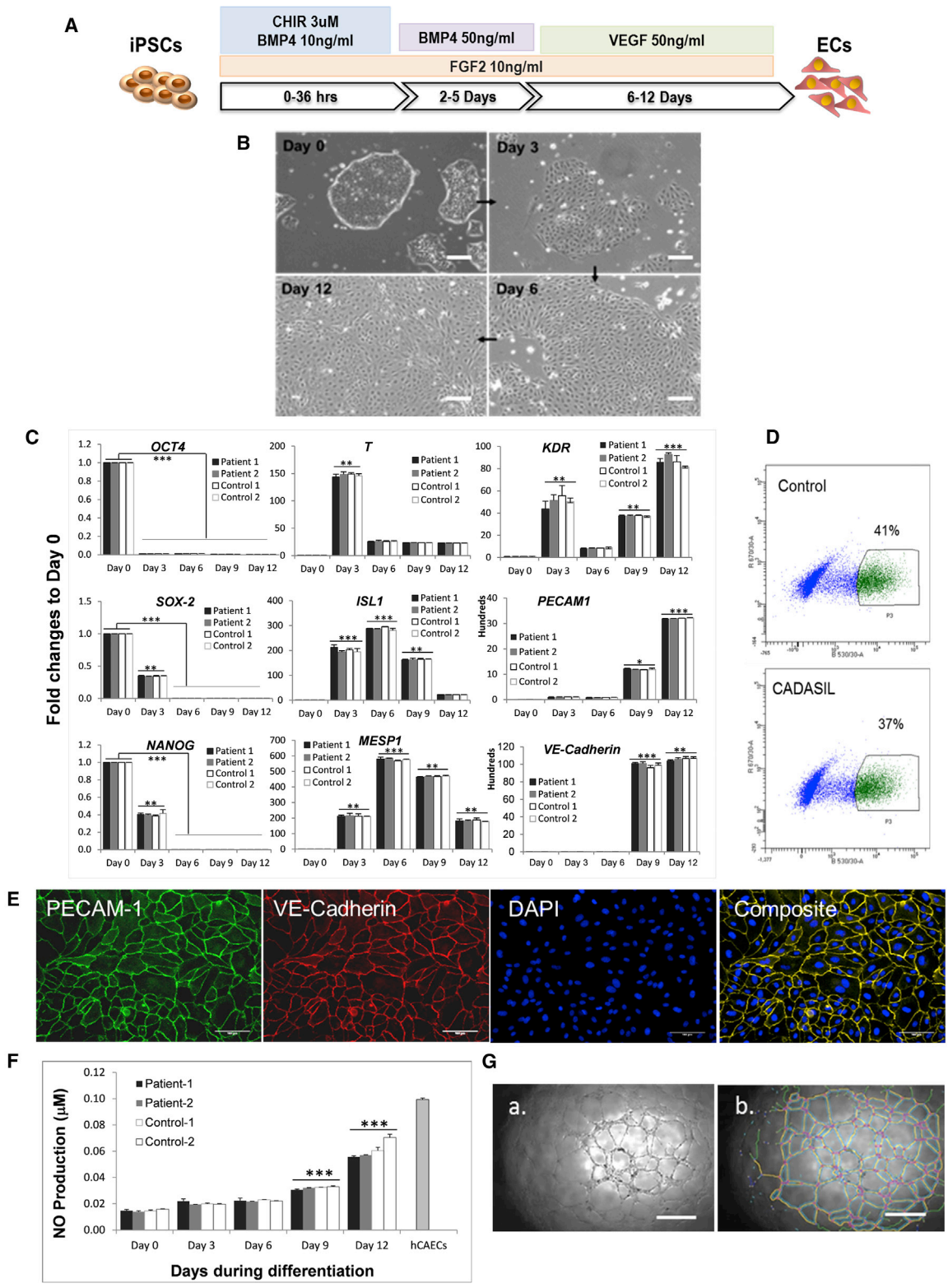

Figure 1. Endothelial Cell Differentiation from iPSCs

(A) Schematic illustration of EC differentiation protocol.

(B) Morphological changes of iPSCs during EC differentiation.

(legend continued on next page)

The whole population of differentiated ECs was then subjected to cell sorting using a VE-cadherin antibody, which revealed the differentiation efficiency to be 37%–45% (Figure 1D). After sorting, a pure population of ECs was obtained and grew healthily after reseeding with expression of endothelial specific marker proteins PECAM-1 and VE-cadherin (Figure 1E).

Functional characterization of the iPSC-ECs showed that the cells progressively gained an ability to produce nitric oxide in response to carbachol treatment during the course of differentiation (Figure 1F). The iPSC-ECs had the ability to form tube-like structures on a Matrigel substrate similar to bona fide endothelial cells, suggesting the generation of functional ECs from iPSCs (Figure 1G).

For MC differentiation, a protocol generating a neuroectoderm intermediate was adopted (Cheung et al., 2012) (Figure 2A) to obtain iPSC-MCs with a phenotype resembling more closely the neural crest-derived MCs in the cerebral arteries where CADASIL pathologies are mainly manifest. In the presence of fibroblast growth factor 2 (FGF2) and the inhibition of transforming growth factor β (TGF-β) type I receptor by SB-431542 for 6–7 days, the iPSCs changed to a bipolar morphology with increased *SOX2* expression and positive SOX1 and Nestin staining. This indicated the production of neural progenitor cells (Figures 2B and 2C). The growth factors were then switched to platelet-derived growth factor BB (PDGF-BB) and TGF-β to specifically promote MC differentiation until day 18 when the cells had adopted a mesenchymal cell-like morphology with significantly increased expression of the SMC markers *α-SMA*, *CNN1*, and *SM22α* (Figures 2B and 2D), and *SMMHC* or *SMTN* (Figure S3).

During EC and MC differentiation, no significant difference was observed between the CADASIL and control iPSCs for the expressions of marker genes tested (Figures 1C and 2B). The expression of *NOTCH3*, *NOTCH1*, *2*, and *4*, NOTCH ligand *JAG1*, and NOTCH target genes *HES1*, *HES2*, and *HEYL* were also not changed in the CADASIL iPSC-MCs (Figure S3). This suggests that *NOTCH3* mutations are unlikely to significantly affect the differentiation of ECs or MCs from iPSCs, or the canonical Notch signaling.

CADASIL MCs Fail to Stabilize Endothelial Capillary Tubule Structure

To address the brain hypoperfusion pathology seen in CADASIL patients, we performed *in vitro* Matrigel-assisted angiogenic network formation using the iPSC-derived vascular cells. When using the iPSC-ECs alone, networks emerged at 6 h after cell seeding, peaked at 24 h, and gradually disassembled and disappeared by 72 h (Figure 3A), representing a typical time course of *in vitro* angiogenesis on Matrigel. There was no significant difference between the CADASIL and control iPSC-ECs in their ability to form networks (Figure 3A), suggesting that the CADASIL *NOTCH3* mutations are unlikely to interfere with *de novo* angiogenesis of ECs. When the control iPSC-MCs were included in the angiogenesis assay, the network structure was significantly stabilized for up to 72 h, reflecting the normal function of MCs in stabilizing capillary structures (Figure 3B). However, when the iPSC-MCs from CADASIL patients were included in the assay, they significantly failed to stabilize the endothelial network (Figure 3B). This observation strongly suggests an intrinsic defect of CADASIL iPSC-MCs.

To confirm the results, we co-cultured CADASIL iPSC-MCs with the control iPSC-ECs and vice versa. Similarly, the CADASIL iPSC-MCs were unable to stabilize the networks formed by the control iPSC-ECs whereas the control iPSC-MCs were able to stabilize the CADASIL iPSC-EC networks (Figure 3C), further suggesting a primary defect of the CADASIL iPSC-MCs.

Accordingly, immunofluorescent imaging showed a clear loss of CADASIL iPSC-MCs from the tubular structures at 24 h after cell seeding, and total disappearance of the iPSC-MCs from the EC network at 48 h (Figure 3D).

To further confirm these results, we used primary SMCs that were isolated from a CADASIL patient and conducted similar *in vitro* angiogenesis assays. In line with findings from the iPSC-MCs, the primary SMCs showed a significant defect in stabilizing the EC networks (Figure S4).

(C) qRT-PCR showing changes of gene-expression profiles for pluripotent (*OCT4*, *SOX2*, *NANOG*), mesodermal (*T*, *ISL-1*, *MESP1*, *KDR*), and endothelial (*KDR*, *PECAM-1*, *VE-CADHERIN*) marker genes relative to GAPDH during the course of iPSC-MC differentiation.

(D) Example of fluorescence-activated cell sorting (FACS) for VE-cadherin$^+$ iPSC-ECs at day 12 of differentiation.

(E) Immunofluorescence staining of VE-cadherin$^+$ iPSC-ECs reseeded after FACS. PECAM-1, green; VE-cadherin, red.

(F) Nitric oxide production from iPSC-ECs over the course of iPSC-EC differentiation compared with that from primary human coronary arterial endothelial cells (hCAECs).

(G) *In vitro* angiogenesis assay in Matrigel showing that iPSC-ECs are able to form capillary tubular networks (a) that are quantifiable for total network length as shown in (b) using ImageJ software.

Data in (C) and (F) are mean ± SEM of three independent experiments (n = 3). Each experiment contained samples from three clones of each CADASIL or control line. Two-way ANOVA with Tukey's post hoc test, *$p \leq 0.05$, **$p \leq 0.01$, ***$p \leq 0.001$, versus day 0; no differences found between CADASIL and controls. Scale bars, 100 μm.

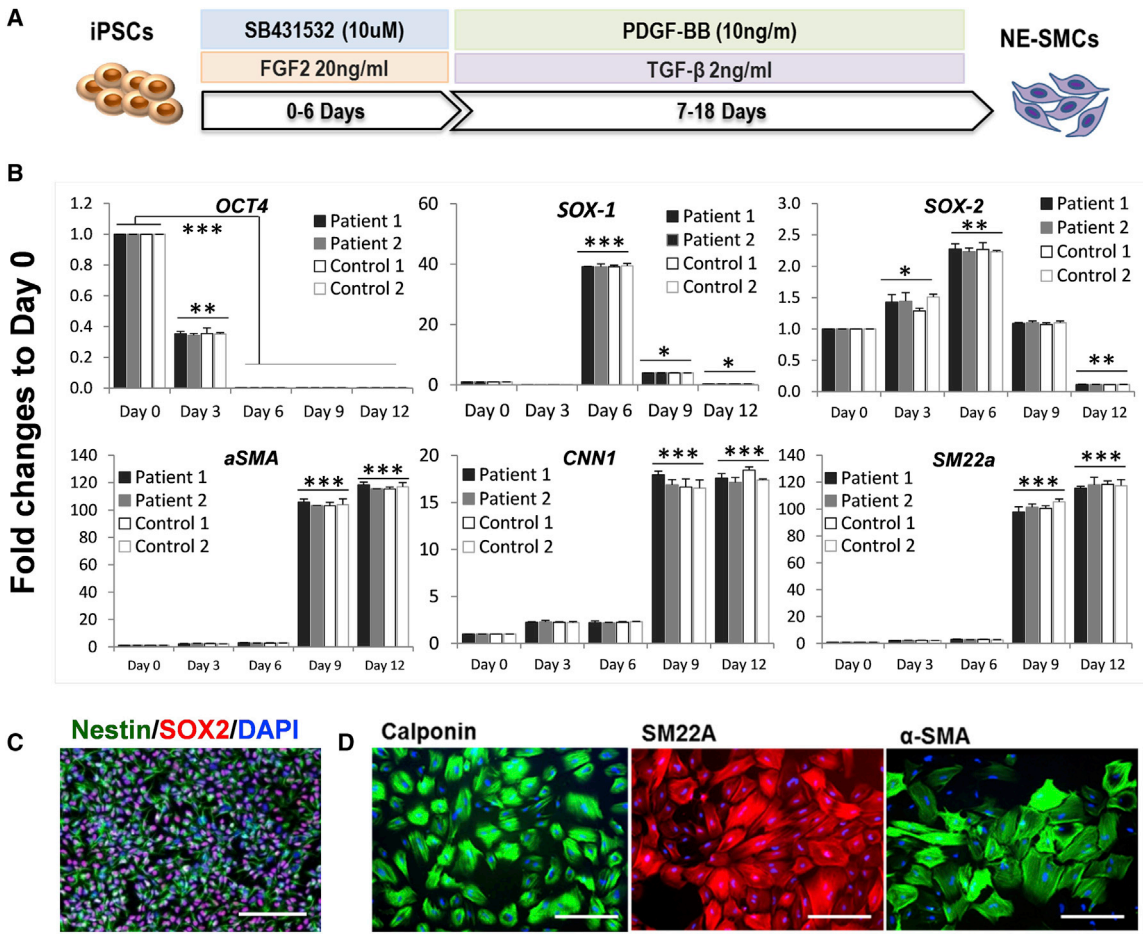

Figure 2. Mural Cell Differentiation from iPSCs through a Neuroectodermal Intermediate

(A) Schematic illustration of MC differentiation protocol.

(B) qRT-PCR determination of gene-expression profiles for the pluripotent (*OCT3/4*), neuroectodermal (*SOX-1*, *SOX-2*), and smooth muscle/MC (*SM22a*, *CNN1*, *α-SMA*) markers during iPSC-MC differentiation. Data are mean ± SEM of three independent experiments (n = 3). Each experiment contained samples from three clones of each CADASIL or control line. There were no differences found between CADASIL and controls. Two-way ANOVA tests was followed by Tukey's post hoc test in (B). *p ≤ 0.05, **p ≤ 0.01, ***p ≤ 0.001 versus day 0. Scale bars, 200 mm (C) and 100 mm (D).

(C) Immunofluorescence staining for neural stem cell marker Nestin (green) and Sox-1 (red) at day 6 of the iPSC-MC differentiation with DAPI nuclear counterstain (blue).

(D) Immunofluorescence staining for SMC markers calponin (green), SM22a (red), and α-SMA (green) at day 18 of differentiation with DAPI counterstaining (blue).

Immunostaining showed that at the 48-h time point, the angiogenic tubule structure had significantly disintegrated and cells formed aggregates in assays that contained CADASIL SMCs (Figure S4B).

An *in vivo* angiogenesis assay in SCID mice was also carried out, by subcutaneous injection of a mixture of the iPSC-ECs and iPSC-MCs from the patient or control with Matrigel. Two weeks after implantation, network structures were formed, mainly by the human iPSC-derived vascular cells, as evidenced by the human-specific mitochondrial antibody staining (Figure S5A). In line with the *in vitro* findings above, the patient iPSC-MCs (calponin$^+$) were extremely sparse in the network structure within the Matrigel plugs (Figures S5Ba, S5Bb, S5Be, and S5Bf). In contrast, control iPSC-MCs were still abundant in the network (Figures S5Bc, S5Bd, S5Bg, and S5Bh), suggesting lack of support of the *in vivo* capillary tubules by CADASIL MCs. Notably, apart from a thin capsule layer formed around the plugs, as indicated by the dense band of DAPI-stained cells lacking anti-human mitochondrial signals, there was no significant host vascular cell invasion into the Matrigel plugs within 2 weeks of implantation (Figure S5A).

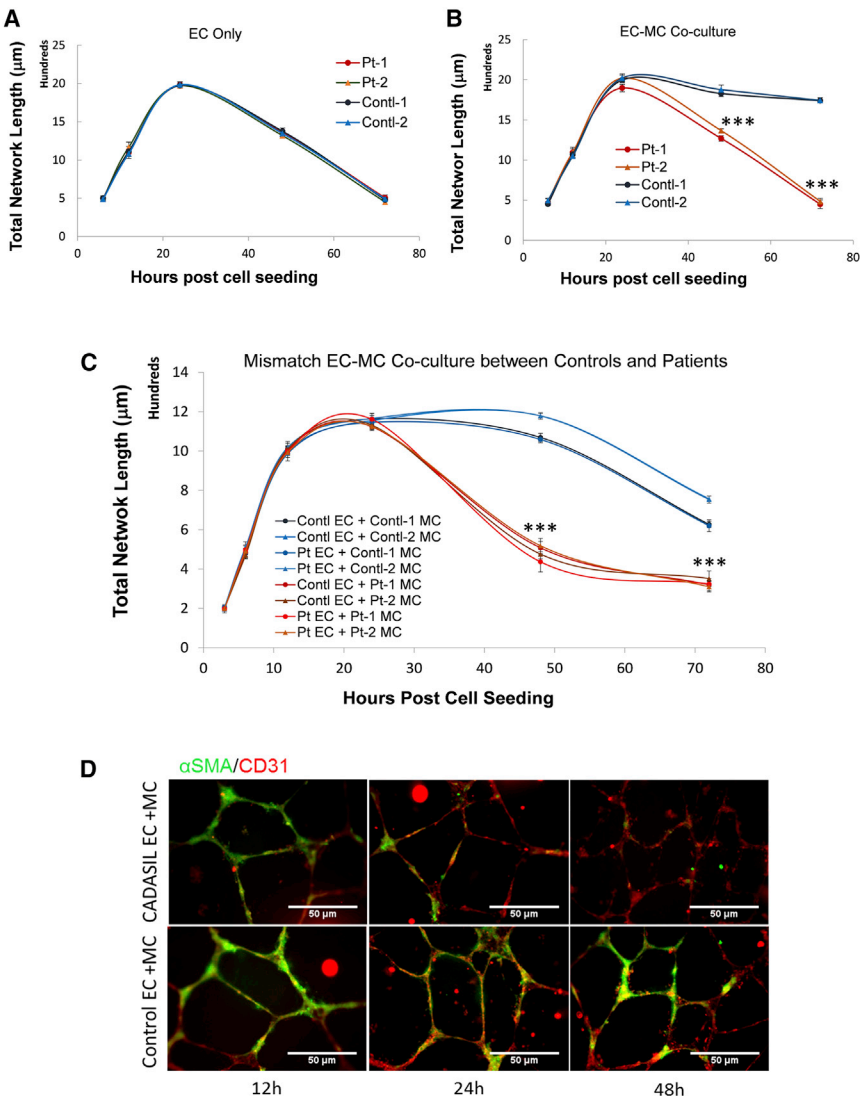

Figure 3. *In Vitro* Angiogenesis Analysis of iPSC-Derived Endothelial Cells and Mural Cells

iPSC-derived ECs and MCs were cultured in Matrigel for *in vitro* assay of capillary tubule network formation.

(A) *In vitro* tubule formation by iPSC-ECs alone. CADASIL samples from two patients are in red and orange, respectively; control samples from two individuals are in blue and green, respectively.

(B) iPSC-ECs co-culture with iPSC-MCs. Result showing CADASIL iPSC-MCs failed to support stability of the tubule structure compared with the controls in the iPSC-EC/MC co-culture.

(C) *In vitro* tubule formation by iPSC-EC/MC co-culture in different combinations of CADASIL and control iPSC-ECs and iPSC-MCs. CADASIL iPSC-MCs had impaired ability to support the tubule stability formed by either CADASIL or control iPSC-ECs (warm colored lines) while the control iPSC-MCs were able to stabilize the tubule structure (cold colored lines).

(D) Immunofluorescence staining of the tubular structures formed by iPSC-EC/MC co-culture showing failure of CADASIL iPSC-MCs (α-SMA, green) to engage with iPSC-ECs (CD31, red) from 24 h onward during the angiogenesis assay.

Data in (A) to (C) are presented as mean ± SEM of three independent experiments (n = 3). Each experiment contained samples from three clones of each CADASIL or three clones of each control line. Two-way ANOVA with Tukey's post hoc test, ***$p < 0.001$. Scale bars, 50 µm.

CADASIL MCs Have Reduced Expression of PDGFRβ

The capillary stability is usually supported by pericytes. This cell type is difficult to distinguish from VSMCs based on marker gene expression alone, but can generally be identified by their ability in supporting capillary structures, and their location and morphology (van Dijk et al., 2015). The iPSC-MCs that we generated were associated with and supported the capillary structures (Figures 3 and S6A), and expressed a combination of commonly used pericyte marker genes (*PDGFRβ*, *NG2*, and *α-SMA*; Figure S6B), fulfilling the current criteria for pericytes. Therefore, the iPSC-MC-assisted angiogenesis could be used as a pericyte model, and the defect of CADASIL iPSC-MCs in supporting the EC network structure suggests a pericyte dysfunction in CADASIL.

PDGFRβ is known to play a key role in pericyte recruitment by ECs and capillary structure maintenance during angiogenesis (Ribatti et al., 2011). We therefore measured *PDGFRβ* level by qRT-PCR and western blotting, and found significant reduction of PDGFRβ in CADASIL iPSC-MCs (Figures S6C and S6D). However, supplement of PDGF was not able to extend the stability of the network formed by iPSC-ECs alone (Figure S6E), suggesting that the presence of the actual PDGFRβ-expressing pericytes is required. Indeed, application of a PDGFR inhibitor did not affect network formation by iPSC-ECs (Figure S6F), confirming that PDGF is not essential for the tubule formation by ECs alone. Additionally, the reduced capillary stabilizing effect by the PDGFRβ-deficient CADASIL iPSC-MCs could not be compensated by simply increasing the PDGFRβ ligand PDGF-BB in the EC-MC co-cultured angiogenesis assay system; instead, PDGF-BB showed a detrimental effect on the tubule stability (Figure S6G), which could be due to the pro-migration role of PDGF (Marmur et al.,

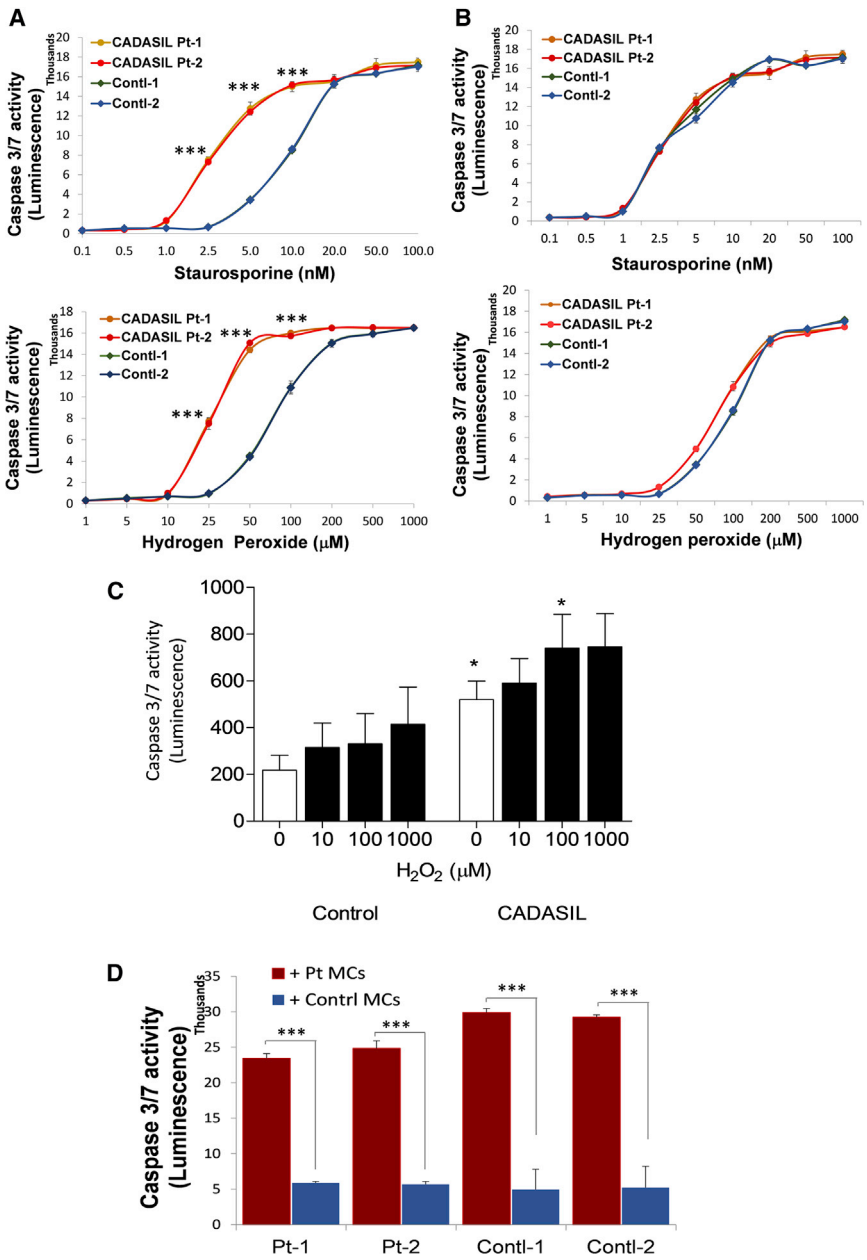

Figure 4. Apoptosis of iPSC-MCs, iPSC-ECs, and Primary SMCs from CADASIL and Control Individuals

(A and B) CADASIL and control iPSC-MCs (A) and iPSC-ECs (B) were exposed to increasing concentrations of staurosporine and hydrogen peroxide for 24 h, and caspase-3/7 activity was then determined by a Promega Caspase-Glo 3/7 Assay Kit. Data are presented as mean ± SEM of three independent experiments (n = 3). Each experiment contained samples from three clones of each CADASIL or three clones of each control line. Two-way ANOVA with Tukey's post hoc test, ***$p \leq 0.001$ versus control samples.

(C) Primary SMCs isolated from small arteries of four CADASIL patients and four control individuals were exposed to increasing concentrations of hydrogen peroxide for 24 h. Caspase-3/7 activity was determined as mentioned above. Data are mean ± SEM, n = 4/group. One-way ANOVA with Bonferroni's post hoc test, *$p < 0.05$ versus control counterparts.

(D) Different combinations of CADASIL and control iPSC-MCs and iPSC-ECs were co-cultured for 24 h, and the iPSC-MCs and iPSC-ECs were then separated by CD31 magnetic beads. Caspase-3/7 activity in the separated iPSC-ECs was determined. Co-cultures of either CADASIL or control iPSC-ECs with CADASIL iPSC-MCs (red); co-culture of either CADASIL or control iPSC-ECs with control iPSC-MCs (blue). Data are mean ± SEM of three independent experiments (n = 3) for each patient or control iPSC lines with three technical repeats for each sample in each experiment. Student's t test, ***$p \leq 0.001$.

1992), resulting in a decreased engagement of MCs with ECs.

CADASIL iPSC-MCs Are Sensitive to Apoptotic Insults and Impair Adjacent EC Survival

The impaired engagement of CADASIL MCs with ECs could also be the result of reduced survival of the CADASIL MCs; therefore, apoptosis was measured using a caspase assay. Under basal states, caspase activity was similarly very low in both CADASIL and control iPSC-MCs (Figure 4A). However, when the cells were challenged by the apoptotic inducers staurosporine and hydrogen peroxide, a significant and dose-dependent increase in apoptosis was induced in the CADASIL iPSC-MCs compared with the control (Figure 4A). In contrast, caspase activity was identical between the iPSC-ECs from CADASIL patients and controls (Figure 4B), which excluded the likelihood of ECs being the primary cause of capillary structure destabilization. The increased sensitivity of CADASIL MCs to apoptotic challenge was further confirmed in primary VSMCs isolated from CADASIL patients (Figure 4C).

Additionally, CADASIL iPSC-MCs exhibited detrimental effects on the adjacent iPSC-ECs. When the iPSC-MCs and iPSC-ECs were co-cultured for 24 h before being

separated using CD31 antibody-conjugated magnetic beads and then subjected to caspase activity determination, the CADASIL iPSC-MCs significantly induced apoptosis of the iPSC-ECs from both CADASIL and control individuals, whereas the control iPSC-MCs did not have such an effect on adjacent iPSC-ECs (Figure 4D).

CADASIL iPSC-MCs Have Reduced Secretion of VEGF

To determine whether soluble factors are involved in the detrimental effect of CADASIL MCs on ECs, we applied conditioned medium from iPSC-MC culture to the iPSC-EC angiogenesis assay. The conditioned medium from CADASIL iPSC-MCs significantly disrupted the angiogenic tubule formation by either control or CADASIL iPSC-ECs (Figures 5A and 5B), suggesting an abnormal secretion of soluble paracrine factor(s) from the CADASIL iPSC-MCs. This was further supported using a transwell co-culture system in which the iPSC-MCs were grown on an insert without direct contact with ECs (Figure 5C). Again the EC-tubule structures collapsed significantly earlier when the CADASIL iPSC-MCs rather than the control iPSC-MCs were present (Figure 5C).

To identify the nature of the soluble factor(s) that were abnormally secreted from the CADASIL iPSC-MCs, we screened an angiogenesis antibody array. A significant reduction in VEGF level was identified in the CADASIL iPSC-MC culture medium (Figures 6A and S7), which was confirmed by quantitative ELISA (Figure 6B) and qRT-PCR on the CADASIL iPSC-MCs (Figure 6C). A trend of reduced mRNA expression and secretion of VEGF was also confirmed on the primary VSMCs that were isolated from a CADASIL patient (Figures 6D and S7).

Supplementing with VEGF Significantly Rescues the Stability of Endothelial Capillary Structures

VEGF is critically involved in angiogenesis. We demonstrated that supplementation of VEGF could promote angiogenesis for both control and CADASIL iPSC-ECs (Figure S7D), and blocking VEGF receptors completely abolished the angiogenesis (Figure S7E). We then supplemented VEGF to the iPSC-EC-MC co-culture angiogenesis assay, which significantly stabilized the tubule structure formed by iPSC-ECs and iPSC-SMCs from CADASIL patients for a further ~48 h (Figure 7A). The exogenous VEGF did not have detectable effects on the tubule structure formed by the co-cultured control iPSC-ECs and iPSC-MCs.

VEGF Secretion from CADASIL iPSC-MCs Was Restored by siRNA Knockdown of *NOTCH3*

To clarify whether the CADASIL phenotype that we identified was caused by loss- or gain-of-function mutation of *NOTCH3*, we used siRNA to knock down the *NOTCH3* transcript in the iPSC-MCs, which achieved 80% knockdown efficiency (Figure 7C). When the NOTCH3-deficient CADASIL iPSC-MCs were co-cultured with iPSC-ECs, the tubule stabilizing ability was significantly restored (Figure 7B), similar to the extent of the VEGF rescue seen in Figure 7A. Accordingly, VEGF in the culture medium of the CADASIL iPSC-MCs returned to the control level after siRNA *NOTCH3* knockdown (Figure 7D), suggesting a gain-of-function phenotype by the mutant NOTCH3. *NOTCH3* knockdown by siRNA did not have a significant impact on the tubule formation by the control iPSC-derived ECs and SMCs.

DISCUSSION

Using a patient-specific iPSC model, we demonstrated an intrinsic defect of vascular MCs in supporting angiogenic capillary structures. The CADASIL MCs could either directly interfere with the stability of the capillary structures formed by ECs, or decrease the secretion of paracrine factors such as VEGF to reduce the tubule stability. This mechanism likely delays the brain tissue repair after stroke in CADASIL patients and contributes to the reduced capillary density and cerebral hypoperfusion in CADASIL brains reported in recent studies (Joutel et al., 2010), and could explain the endothelial phenotype reported in CADASIL arteries.

CADASIL is a typical dominant single-gene disorder. To date, more than 200 different mutations in the *NOTCH3* gene have been documented in the Human Gene Mutation Database, the majority of which are missense mutations. Although there is no significant genotype-phenotype correlation in the clinical cases and disease severity varies among members from the same family, mutations in the *NOTCH3* gene are highly stereotypical. Almost all CADASIL mutations fall within the EGF repeats of the extracellular domain of the NOTCH3 protein, which gives rise to loss or gain of a cysteine amino acid resulting in odd numbers of cysteines in a given EGF repeat (Joutel et al., 1997). As a result, CADASIL pathologies in the vasculature are unique and consistent across the spectrum of different mutations. Additionally, about 70% of all CADASIL mutations are clustered in exons 3 and 4 of the *NOTCH3* gene (Joutel et al., 1997), suggesting the importance of the N-terminal region of the protein in disease pathology. The iPSCs used in our study were generated from two CADASIL patients carrying mutations Arg153Cys and Cys224Tyr, respectively. Both mutations locate within exon 4 of the *NOTCH3* gene, with one mutation creating gain of a cysteine residue (Arg153Cys) and the other loss of a cysteine (Cys224Tyr). These are representative of common CADASIL mutations. The two CADASIL patients also had

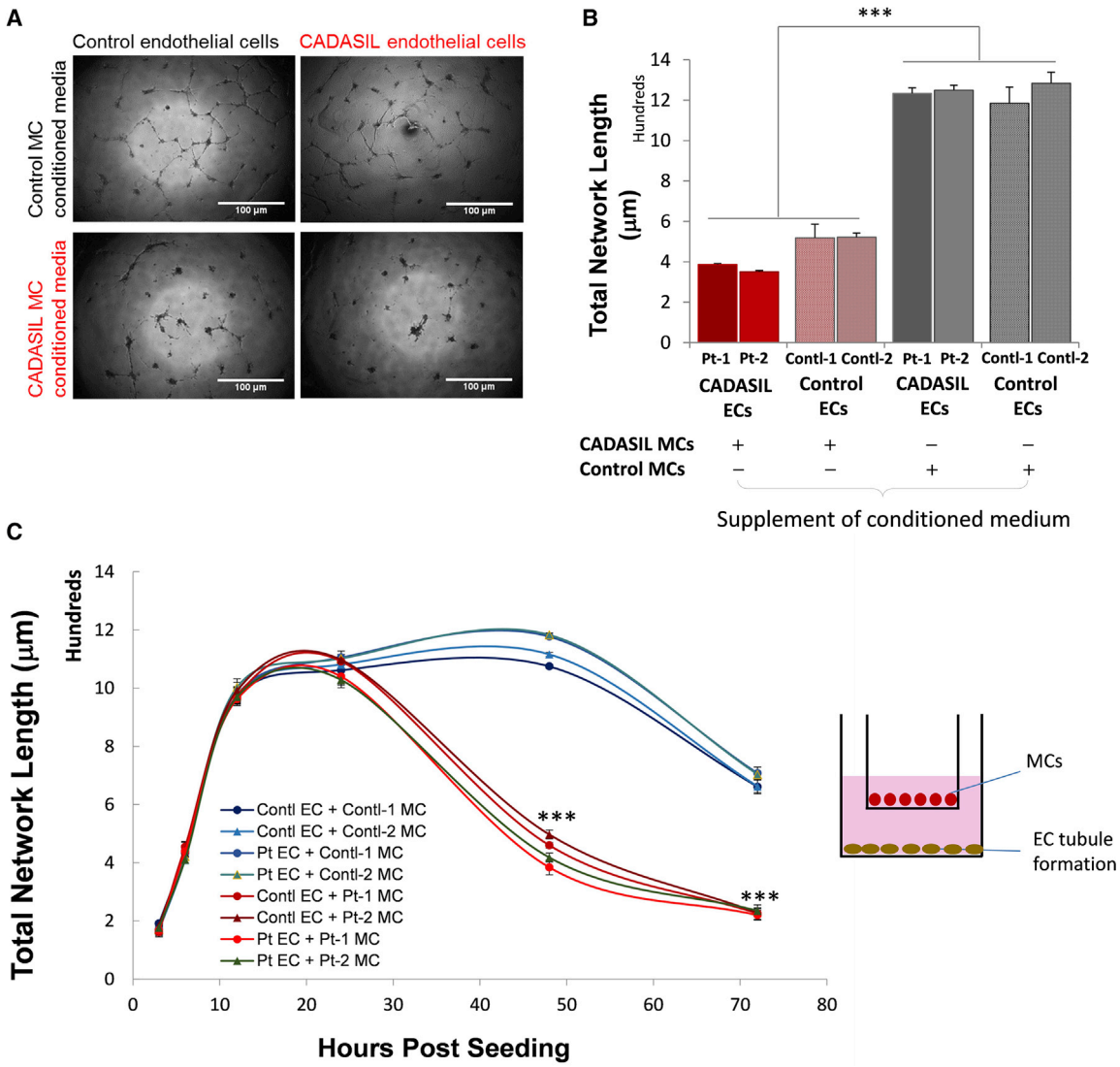

Figure 5. Effect of iPSC-MC-Secreted Soluble Factors on iPSC-EC Angiogenesis

(A) Images of *in vitro* iPSC-EC angiogenesis assay in the presence of conditioned medium from CADASIL or control iPSC-MCs for 24 h. Scale bars, 100 µm.

(B) Quantification of total network length of iPSC-EC *in vitro* angiogenesis assays when cultured with conditioned media from CADASIL or control iPSC-MCs 24 h after cell seeding.

(C) *In vitro* angiogenesis assay in a transwell setup of iPSC-EC/MC co-culture where iPSC-ECs were cultured on the bottom of the well and iPSC-MCs on the surface of the insert, as shown by the diagram on the right.

Data in (B) and (C) are presented as mean ± SEM of three independent experiments (n = 3). Each experiment contained samples from three clones of each CADASIL or three clones of control lines. One-way (B) or two-way (C) ANOVA with Tukey's post hoc test, ***$p \leq 0.001$ versus controls.

typical clinical manifestations, e.g., recurrent strokes and cognitive decline, which represent the common phenotypes of the CADASIL cohort.

In our study, the "footprint-free" reprogramming with SeV was used, which has avoided post-transfection genome perturbation, making the iPSC disease model more physiological. One of the two control iPSC lines was from the sibling of one patient, which has minimized the genetic background variation. Most importantly, key findings from CADASIL iPSCs were recapitulated in primary VSMCs isolated from small arteries of skin biopsies of CADASIL patients (Figures S4, 4C, and 6D). However, with respect to the control primary VSMCs, due to the limited availability of the skin biopsy, we have used primary human coronary

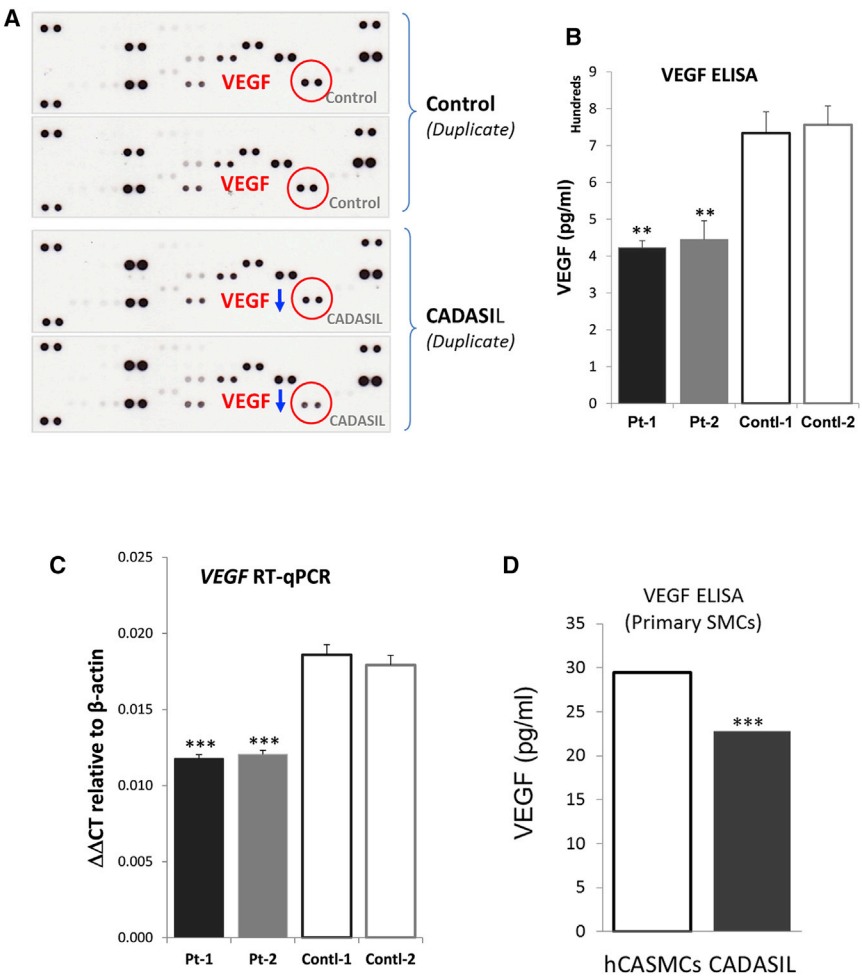

Figure 6. Identification of Abnormal Paracrine Factors Secreted from the CADASIL iPSC-MCs

(A) Angiogenesis Proteome Profiler Array (R&D Systems) was screened using conditioned media from CADASIL and control iPSC-MCs. VEGF (red circles) was identified as downregulated (blue arrows) in conditioned media of CADASIL iPSC-MCs.

(B) ELISA quantitation of VEGF in the conditioned media of iPSC-MCs.

(C) qRT-PCR quantitation of VEGF in iPSC-MCs. Data in (B) and (C) are mean ± SEM of three independent experiments (n = 3). Each experiment contained samples from three clones of each CADASIL or three clones of each control line.

(D) VEGF secretion from primary SMCs isolated from a CADASIL patient. Equal numbers of primary SMCs from small arteries of CADASIL patients and healthy human coronary arteries (hCASMCs, control) were seeded in serum-free medium for 3 days. VEGF-165 levels in the conditioned medium were measured by ELISA assay and normalized to the final cell numbers in each well. Data are mean ± SEM from three independent experiments. Unpaired Student's t test, ***$p \leq 0.001$.

artery smooth muscle cells (hCASMCs) that are derived from small vessels (coronary arteries) of healthy individuals for some of the experiments (Figures S4 and 6D). As small arteries rather than large conduit arteries are typically involved in CADASIL, we consider that the hCASMCs from "normal" subjects (i.e., without CADASIL and *NOTCH3* mutations) are appropriate as control human non-CADASIL cells. Nevertheless, in future work we hope to entirely eliminate the influence of genetic background by introducing isogenic control iPSC lines.

Based on knowledge of endothelial differentiation during embryonic development, we optimized a chemically defined highly reproducible protocol for EC differentiation. This protocol gave >40% differentiation efficiency, from which pure populations of ECs were obtained by VE-cadherin cell sorting. This EC differentiation protocol was not designed to generate brain-specific microvascular endothelial cells that possess barrier functions. Given the fact that barrier genesis in the brain is a process that follows the primary angiogenic vascular network formation, the iPSC-ECs used in our study likely reflect an early general angiogenesis process. For MC differentiation, we adopted a neuroectoderm-specific VSMC differentiation protocol described by Cheung et al. (2012). The wild-type iPSC-MCs obtained in our study exhibited a typical pericyte function in supporting EC capillary structures. Pericytes and VSMCs are vascular MCs, with the former specifically located directly on the capillary wall and the latter sitting in the middle layer of muscular vessels and arterioles. Both cell types originate from either mesoderm or neural crest (neuroectoderm) during embryonic development and share marker genes, making them difficult to distinguish without functional assays (Winkler et al., 2011). However, a more recent study using single-cell RNA sequencing on mouse brain vasculature (Vanlandewijck et al., 2018) demonstrated that *PDGFRβ* and *NG2* were expressed in both SMCs and pericytes, whereas *α-SMA*, *CNN1*, and *SM22* were only expressed in SMCs and not in pericytes. On the other hand, recent publications have also noticed that when pericytes, including human primary pericytes, were put in cell culture, they consistently expressed *α-SMA* (Alarcon-Martinez et al., 2018; Smyth

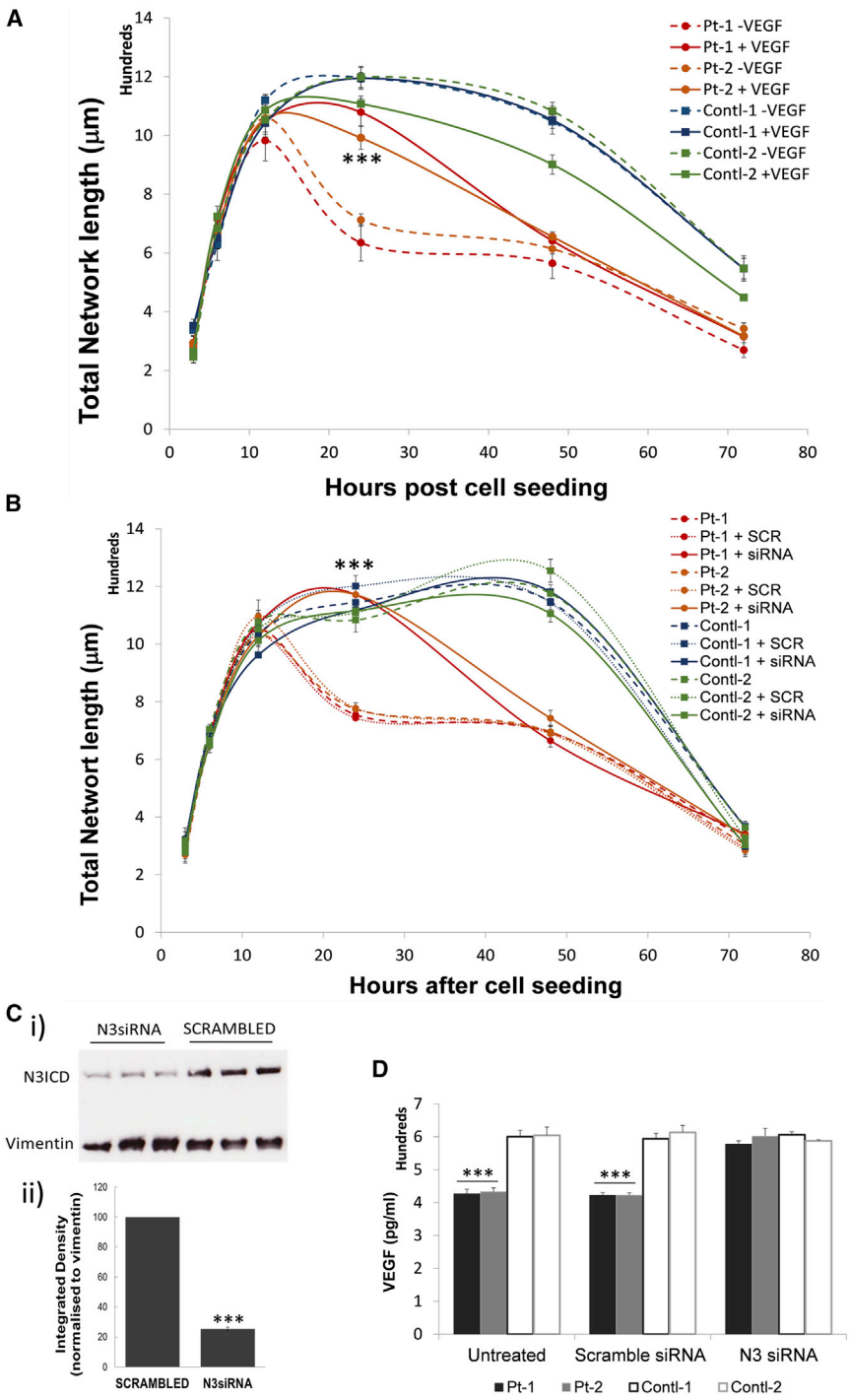

Figure 7. Phenotype Rescue of the Defective iPSC-EC/MC Tubule Stability by Exogenous VEGF or siRNA Knockdown of *NOTCH3* in iPSC-MCs

(A) *In vitro* angiogenic tubule formation by co-culture of iPSC-ECs/MCs on Matrigel was carried out in the presence or absence of 20 ng/mL recombinant VEGF-165.

(B) *In vitro* angiogenic tubule formation was carried out by co-culture of iPCS-ECs/MCs with *NOTCH3* knocked down in iPSC-MCs by siRNA.

(C) Confirmation of siRNA knockdown of *NOTCH3* by western blotting (i). The quantification of the western blotting results is shown in (ii). Data are integrated density relative to the protein loading control vimentin, and presented as mean ± SEM. Shown are example results from one of the iPSC clones and three independent siRNA knockdown samples. Student's t test, ***p $\leq$ 0.001.

(D) VEGF was quantified in the conditioned medium from CADASIL or control iPSC-MCs after siRNA *NOTCH3* knockdown.

Data are presented as mean ± SEM of three independent experiments (n = 3). Each experiment contained samples from three clones of each CADASIL or three clones of each control line. Two-way ANOVA and Turkey's post hoc test, ***p $\leq$ 0.001 versus non-treated samples (A and B), or versus control samples (D). Scrambled was the control siRNA.

et al., 2018; Stebbins et al., 2019; Yao et al., 2014). Possible explanations include the culture conditions, e.g., the use of serum (Rustenhoven et al., 2016; Tigges et al., 2012), proliferation status (Rustenhoven et al., 2016), the lack of laminin (Yao et al., 2014), or the detection method (Alarcon-Martinez et al., 2018). Three contractile markers, *α-SMA*, *CNN1*, and *SM22α*, were found to be expressed in human primary pericytes (Stebbins et al., 2019). It seems that the expressions of *α-SMA*, *CNN1*, and *SM22α* seen under *in vitro* cell-culture conditions do not necessarily rule out the pericyte-like nature of the iPSC-derived MCs. Of prime importance is that the cells recapitulate key functional attributes of pericytes. The iPSC-MCs in our study expressed key pericyte markers, *PDGFRβ* and *NG2*, in

addition to the capillary supporting function, suggesting that they represent an *in vitro* pericyte-like model that can be used for angiogenesis assays independent of a VSMC model. The iPSC-MCs derived via the neuroectoderm lineage were more closely representative of MCs in the cerebral vasculature, where the CADASIL pathology mainly resides, than iPSC-MCs differentiated via a mesodermal lineage (data not shown).

During angiogenesis, pericytes are recruited via cell-surface receptor PDGFRβ to the nascent capillary tubule by the soluble ligand PDGF-BB secreted locally from the tip of endothelial sprouts. This, together with other regulators such as ANG1-TIE2 signaling, supports the capillary stability (Phng and Gerhardt, 2009; Ribatti et al., 2011). Such function is more likely perturbed due to the loss of PDGFRβ in the CADASIL iPSC-MCs, although we did not directly demonstrate this process. This is supported by a recent publication based on PDGFRβ immunostaining where reduction of pericyte numbers was observed in a CADASIL transgenic mouse model (Ghosh et al., 2015). We did not find any change in *TIE2* expression in the CADASIL MCs, suggesting that ANG1-TIE2 signaling is unlikely involved in the impaired capillary structural stability in CADASIL. NOTCH3 is important for the establishment of brain vascular integrity by regulating pericyte numbers and for the investment of MCs in angiogenesis (Henshall et al., 2015; Wang et al., 2014). Such a function is likely perturbed by the *NOTCH3* mutations in CADASIL.

In the central nervous system, pericytes also play a central role in the regulation of capillary diameter, which controls pressure-induced autoregulation of cerebral blood flow (CBF) (Winkler et al., 2011). Reduced CBF has already been observed in CADASIL patients, and pressure-induced regulation of myogenic tone was found to be impaired in a CADASIL mouse model (Hussain et al., 2004; Lacombe et al., 2005). Evidence from the mouse model also suggested that brain capillary rarefaction contributes to CBF reduction (Joutel et al., 2010). Therefore, dysfunction of pericyte-like cells found in our study could likely be a key mechanism contributing to the cerebral vascular phenotype in CADASIL individuals.

VEGF is a critical factor that drives and guides angiogenesis (Herbert and Stainier, 2011). VEGF secreted by pericytes also acts in a juxtacrine/paracrine manner as a survival and stabilizing factor for ECs in microvessels (Darland et al., 2003). A recent study demonstrated that VEGF enhanced pericyte coverage of brain ECs via mechanisms involving increased N-cadherin expression on cerebral microvessels (Zechariah et al., 2013). It is therefore not difficult to understand the impaired stabilization of the capillary structures by the CADASIL iPSC-MCs with reduced secretion of VEGF in our study. Once MCs are recruited to the angiogenic stalks, VEGF levels are locally reduced to support the establishment of quiescence of the capillary structure. Excess VEGF at this stage could promote EC migration, leading to tubule instability. This could partially explain the incomplete rescue of the angiogenic phenotype by supplementing VEGF in this study, in addition to the impaired direct interactions between CADASIL MCs and ECs. While we have focused on VEGF in the present study, data from the angiogenesis proteome profiler arrays screen suggest that many other factors may also be important and warrant further investigation.

It is known that CADASIL *NOTCH3* mutations do not usually disrupt the RBP-Jκ-mediated canonical Notch signaling, since in Notch3$^{-/-}$ mice crossed with CADASIL transgenic mice, activation of RBP-Jκ was restored, suggesting that CADASIL *NOTCH3* mutations are not loss-of-function mutations (Monet et al., 2007). However, it is not known whether the mutations lead to loss of an as yet unidentified NOTCH3 function, which has not been investigated due to limitations of the existing models. Using siRNA knockdown of *NOTCH3* in the CADASIL iPSC-derived MCs, the phenotype of impaired angiogenic tubule stability was significantly rescued to a similar extent as when VEGF was supplemented (Figures 7A and 7B). This was accompanied with a full restoration of VEGF secretion (Figure 7D), suggesting a gain-of-function mechanism. The nature of the neomorphic function awaits further investigation but is unlikely through the activation of the canonical Notch signaling, as neither *NOTCH3* expression nor its target genes were changed in the CADASIL iPSC-MCs (Figure S3). Furthermore, knockdown of *NOTCH3* in the control MCs did not give rise to the same angiogenic phenotype seen in CADASIL MCs, confirming that the impaired angiogenic tubule stability was not via a loss-of-function mechanism through the mutant NOTCH3.

In conclusion, we have established a patient-specific iPSC model for CADASIL, the most common type of genetic stroke and vascular dementia syndrome. The iPSCs were successfully differentiated into ECs and MCs. Functional characterizations of the iPSC-derived vascular cells revealed significant failure of the CADASIL MCs to support angiogenic capillary structures, maintain EC survival, and secrete angiogenic paracrine factors. Key findings from the iPSC model were also confirmed in primary VSMCs isolated from CADASIL patients. The novel mechanisms we have identified will help to unravel the contribution of vascular factors to cerebral pathologies in CADASIL and related diseases and identify drug targets. The phenotype and the iPSC model could be used for high-throughput screening of potential therapeutic molecules for future treatment of CADASIL.

EXPERIMENTAL PROCEDURES

Please see Supplemental Information for details of the methods.

Establishment of Patient-Derived iPSCs

Dermal fibroblasts were isolated from skin biopsies of two CADASIL patients carrying *NOTCH3* Arg153Cys and Cys224Tyr mutations, respectively, and a non-affected control individual under a local ethical approval (REC reference no. 12/NW/0533). Adult HDFs were purchased from Invitrogen as an additional non-CADASIL control. The HDFs were reprogrammed into iPSCs using the Cytotune-iPSC 2.0 kit (Life Technologies) according to the manufacturer's instructions. Twenty-eight days after the SeV-mediated delivery of *OCT*, *SOX-2*, *KLF4*, and *C-MYC*, positive iPSC colonies were identified, excised, and cultured in Essential 8 medium (E8; Life Technologies) on vitronectin (VTN-N)-coated (Life Technologies) 6-well plates. Selected iPSC clones were karyotyped and *NOTCH3* mutations were confirmed by Sanger DNA sequencing.

Endothelial Cell Differentiation from iPSCs

iPSCs were seeded onto a VTN-N-coated 6-well plate at around 1 cell cluster (10–20 cells) per cm^2 and cultured for 24 h at 37°C in E8 containing 10 μM Y-27632 followed by a further 24-h culture without Y-27632. The cells were then cultured in Essential 6 medium (E6; Life Technologies) supplemented with 3 μM CHIR99021 (Calbiochem), 10 ng/mL recombinant BMP4 (Peprotech), and 10 ng/mL recombinant FGF2 (Peprotech). After a further 24 h of culture, the medium was replaced with E6 supplemented with 50 ng/mL BMP4 and 10 ng/mL FGF2, and renewed every 24 h. On day 7 of differentiation, BMP was reduced to 25 ng/mL, and 25 ng/mL VEGF-165 (Peprotech) was included in the medium. The cells were cultured for a further 24 h before VEGF-165 was increased to 50 ng/mL and BMP4 was withdrawn. The medium was replaced every 24 h until day 12 of differentiation. A pure population of iPSC-ECs was then obtained by fluorescence-activated cell sorting using PE-conjugated human VE-cadherin antibody (R&D Systems).

Mural Cell Differentiation from iPSCs

MC differentiation via a neuroectoderm lineage was adapted from Cheung et al. (2012). In brief, iPSCs were seeded on VTN-N-coated 6-well plates at around 1–2 clusters/cm^2 in E8 supplemented with 10 μM of Y-27632 and cultured for 24 h before switching to E6 that contained 10 μM SB-431542 (Sigma-Aldrich) and 10 ng/mL FGF2. The medium was replaced every 24 h until day 6 when the supplements were replaced with 2 ng/mL TGF-β (Peprotech) and 5 ng/mL PDGF-BB (Peprotech). The medium was refreshed every 24 h until day 18 of differentiation.

Primary Culture Vascular Smooth Muscle Cells from Patients with CADASIL

To validate our findings in iPSCs, we conducted some experiments, particularly angiogenesis and apoptosis experiments, in primary cultured VSMCs from clinically phenotyped patients with CADASIL. Cells from four CADASIL patients (mutations Arg169Cys, Arg141Cys, and Arg54Cys) and four controls were used between passages 2 and 6.

Reverse-Transcription qPCR

Total RNA was extracted from cells using the RNeasy mini kit (Qiagen) according to the manufacturer's instructions and reverse transcribed to cDNA using a Tetro cDNA synthesis kit (Bioline). Standard qPCR was carried out using SYBR Green reagent (Applied Biosystems; Thermo Scientific). All samples were analyzed in triplicate.

Immunofluorescence Staining and Western Blotting

Immunofluorescence staining and western blotting were performed as described previously (Wang et al., 2007).

Angiogenesis Assay

Ten thousand iPSC-derived iPSC-ECs or a mixture of 1×10^4 iPSC-ECs and 0.5×10^4 iPSC-MCs were plated onto a thin layer of Matrigel in 96-well plates in E6 supplemented with 5 ng/mL VEGF-165 and 2 ng/mL FGF2, and cultured in a CO_2 incubator at 37°C for 3, 6, 12, 24, 48, and 72 h, respectively, for capillary network formation. Results were quantified using ImageJ software.

The *in vivo* angiogenesis assay was performed according to protocols approved by the Institutional Committee for Use and Care of Laboratory Animals (Kings College, London). One hundred microliters containing differentiated iPSC-MCs and iPSC-ECs (1×10^6 cells per sample) was injected subcutaneously into the back or flank of NOD.CB17-*Prkdc*^{scid}/NcrCrl mice. Six injections were conducted for each group. Fourteen days later, the Matrigel plugs were harvested, frozen in liquid nitrogen, and cryosectioned for immunostaining.

Angiogenesis Proteome Profiler Array Analysis and ELISA

The Proteome Profiler Human Angiogenesis Array Kit (ARY007, R&D Systems) was used to screen angiogenesis-related proteins secreted from the control and CADASIL iPSC-MCs in the conditioned medium according to the manufacturer's protocol. Results were confirmed by ELISA assays using a Human VEGF Quantikine ELISA kit (R&D Systems). All samples were analyzed in triplicate.

Apoptosis Assay

The apoptosis of iPSC-MCs and iPSC-ECs was measured using the Caspase-Glo 3/7 Assay kit (Promega). All samples were analyzed in triplicate.

Nitric Oxide Measurement

Nitric oxide concentration in the cell-culture medium was quantified using the Griess Reagent System (Promega). All samples were analyzed in duplicate.

Small Interfering RNA *NOTCH3* Knockdown in iPSC-MCs

Notch3-specific siRNA sequences and a scrambled negative control siRNA were purchased from Qiagen (Venlo, Netherlands) and delivered to iPSC-MCs by the 4D-nucleofector system (AAF-1002B+ X unit) (Lonza) using the 4D p3 kit (Lonza) with program CM138.

Statistics

Gaussian distribution of each dataset was determined by the Shapiro-Wilks test. Data were presented as mean ± SEM. The unpaired Student's t test was used to compare differences between results from two groups of samples. Where more than two means were compared, one-way or two-way ANOVA in conjunction with Tukey's post hoc test or Bonferroni's post hoc test were performed. A p value of ≤ 0.05 was considered statistically significant.

SUPPLEMENTAL INFORMATION

Supplemental Information can be found online at https://doi.org/10.1016/j.stemcr.2019.10.004.

AUTHOR CONTRIBUTIONS

T.W., S.J.K., and J.K. designed the experiments with contributions from Q.X. and P.S. A.D. produced and validated the iPSCs with help from S.J.K. and C.W. J.K. performed most of the iPSC-related experiments including iPSC differentiation and phenotypic characterization. Y.H. and J.K. performed *in vivo* angiogenesis assays. R.M.T. and A.H. provided the primary SMCs from CADASIL patients, and A.H. performed apoptosis assays, S.C. performed *in vitro* angiogenesis assays, and J.R. performed VEGF ELISA on these cells. J.R. and W.Z. performed qRT-PCR on SMMHC and SMTN. N.B. performed immunostaining on the *in vivo* angiogenesis sections. P.S. recruited CADASIL patients for iPSC generation. F.C.M. and K.W.M. recruited CADASIL patients for primary SMC isolation. T.W., J.K., and S.J.K. analyzed the data and wrote the manuscript with contributions from Q.X., R.M.T., P.S., and all other authors.

ACKNOWLEDGMENTS

The study is mainly funded by the British Heart Foundation (BHF) (PG/12/31/2952) and the National Centre for the Replacement, Reduction and Refinement of Animals in Research (NC3Rs, NC/K001744/1). The work is also supported by MRC UK Regenerative Medicine Platform funding (MR/K026666/1), the Stroke Association, and an MRC Confidence in Concept grant. R.M.T. is supported by a BHF Chair and BHF Award of Excellence (CH/12/4/29762; RE/13/5/30177). We thank Dr. Helen Murphy and Iris Trender-Gerhard from Manchester Centre for Genomic Medicine (MCGM) for help in recruiting and biopsying CADASIL patients, and Meenakshi Minnis and Stephen Trueman of MCGM for help in growing HDFs and karyotyping iPSCs. We also thank Drs. Karla Neves and Augusto Montezano, Institute of Cardiovascular and Medical Sciences, Glasgow, for helping with the CADASIL cell culture, and Dr. Paul Rocchicciolli, Golden Jubilee National Hospital, Glasgow, for helping with the biopsies from CADASIL patients.

Received: July 20, 2018
Revised: October 4, 2019
Accepted: October 5, 2019
Published: October 31, 2019

REFERENCES

Alarcon-Martinez, L., Yilmaz-Ozcan, S., Yemisci, M., Schallek, J., Kilic, K., Can, A., Di Polo, A., and Dalkara, T. (2018). Capillary pericytes express alpha-smooth muscle actin, which requires prevention of filamentous-actin depolymerization for detection. Elife *7*. https://doi.org/10.7554/eLife.34861.

Artavanis-Tsakonas, S., Rand, M.D., and Lake, R.J. (1999). Notch signaling: cell fate control and signal integration in development. Science *284*, 770–776.

Bentley, P., Wang, T., Malik, O., Nicholas, R., Ban, M., Sawcer, S., and Sharma, P. (2011). CADASIL with cord involvement associated with a novel and atypical NOTCH3 mutation. J. Neurol. Neurosurg. Psychiatry *82*, 855–860.

Cheung, C., Bernardo, A.S., Trotter, M.W., Pedersen, R.A., and Sinha, S. (2012). Generation of human vascular smooth muscle subtypes provides insight into embryological origin-dependent disease susceptibility. Nat. Biotechnol. *30*, 165–173.

Darland, D.C., Massingham, L.J., Smith, S.R., Piek, E., Saint-Geniez, M., and D'Amore, P.A. (2003). Pericyte production of cell-associated VEGF is differentiation-dependent and is associated with endothelial survival. Dev. Biol. *264*, 275–288.

Domenga, V., Fardoux, P., Lacombe, P., Monet, M., Maciazek, J., Krebs, L.T., Klonjkowski, B., Berrou, E., Mericskay, M., Li, Z., et al. (2004). Notch3 is required for arterial identity and maturation of vascular smooth muscle cells. Genes Dev. *18*, 2730–2735.

Dubroca, C., Lacombe, P., Domenga, V., Maciazek, J., Levy, B., Tournier-Lasserve, E., Joutel, A., and Henrion, D. (2005). Impaired vascular mechanotransduction in a transgenic mouse model of CADASIL arteriopathy. Stroke *36*, 113–117.

Ghosh, M., Balbi, M., Hellal, F., Dichgans, M., Lindauer, U., and Plesnila, N. (2015). Pericytes are involved in the pathogenesis of cerebral autosomal dominant arteriopathy with subcortical infarcts and leukoencephalopathy. Ann. Neurol. *78*, 887–900.

Henshall, T.L., Keller, A., He, L., Johansson, B.R., Wallgard, E., Raschperger, E., Mäe, M.A., Jin, S., Betsholtz, C., and Lendahl, U. (2015). Notch3 is necessary for blood vessel integrity in the central nervous system. Arterioscler. Thromb. Vasc. Biol. *35*, 409–420.

Herbert, S.P., and Stainier, D.Y. (2011). Molecular control of endothelial cell behaviour during blood vessel morphogenesis. Nat. Rev. Mol. Cell Biol. *12*, 551–564.

Hussain, M.B., Singhal, S., Markus, H.S., and Singer, D.R. (2004). Abnormal vasoconstrictor responses to angiotensin II and noradrenaline in isolated small arteries from patients with cerebral autosomal dominant arteriopathy with subcortical infarcts and leukoencephalopathy (CADASIL). Stroke *35*, 853–858.

Joutel, A. (2011). Pathogenesis of CADASIL: transgenic and knockout mice to probe function and dysfunction of the mutated gene, Notch3, in the cerebrovasculature. Bioessays *33*, 73–80.

Joutel, A., Corpechot, C., Ducros, A., Vahedi, K., Chabriat, H., Mouton, P., Alamowitch, S., Domenga, V., Cécillion, M., Marechal, E., et al. (1996). Notch3 mutations in CADASIL, a hereditary adult-onset condition causing stroke and dementia. Nature *383*, 707–710.

Joutel, A., Vahedi, K., Corpechot, C., Troesch, A., Chabriat, H., Vayssiere, C., Cruaud, C., Maciazek, J., Weissenbach, J., Bousser, M.G., et al. (1997). Strong clustering and stereotyped nature of Notch3 mutations in CADASIL patients. Lancet *350*, 1511–1515.

Joutel, A., Andreux, F., Gaulis, S., Domenga, V., Cecillon, M., Battail, N., Piga, N., Chapon, F., Godfrain, C., and Tournier-Lasserve,

E. (2000). The ectodomain of the Notch3 receptor accumulates within the cerebrovasculature of CADASIL patients. J. Clin. Invest. *105*, 597–605.

Joutel, A., Monet, M., Domenga, V., Riant, F., and Tournier-Lasserve, E. (2004). Pathogenic mutations associated with cerebral autosomal dominant arteriopathy with subcortical infarcts and leukoencephalopathy differently affect Jagged1 binding and Notch3 activity via the RBP/JK signaling Pathway. Am. J. Hum. Genet. *74*, 338–347.

Joutel, A., Monet-Lepretre, M., Gosele, C., Baron-Menguy, C., Hammes, A., Schmidt, S., Lemaire-Carrette, B., Domenga, V., Schedl, A., Lacombe, P., et al. (2010). Cerebrovascular dysfunction and microcirculation rarefaction precede white matter lesions in a mouse genetic model of cerebral ischemic small vessel disease. J. Clin. Invest. *120*, 433–445.

Lacombe, P., Oligo, C., Domenga, V., Tournier-Lasserve, E., and Joutel, A. (2005). Impaired cerebral vasoreactivity in a transgenic mouse model of cerebral autosomal dominant arteriopathy with subcortical infarcts and leukoencephalopathy arteriopathy. Stroke *36*, 1053–1058.

Liu, H., Kennard, S., and Lilly, B. (2009). NOTCH3 expression is induced in mural cells through an autoregulatory loop that requires endothelial-expressed JAGGED1. Circ. Res. *104*, 466–475.

Liu, H., Zhang, W., Kennard, S., Caldwell, R.B., and Lilly, B. (2010). Notch3 is critical for proper angiogenesis and mural cell investment. Circ. Res. *107*, 860–870.

Marmur, J.D., Poon, M., Rossikhina, M., and Taubman, M.B. (1992). Induction of PDGF-responsive genes in vascular smooth muscle. Implications for the early response to vessel injury. Circulation *86*, III53–III60.

Monet, M., Domenga, V., Lemaire, B., Souilhol, C., Langa, F., Babinet, C., Gridley, T., Tournier-Lasserve, E., Cohen-Tannoudji, M., and Joutel, A. (2007). The archetypal R90C CADASIL-NOTCH3 mutation retains NOTCH3 function in vivo. Hum. Mol. Genet. *16*, 982–992.

Peters, N., Opherk, C., Zacherle, S., Capell, A., Gempel, P., and Dichgans, M. (2004). CADASIL-associated Notch3 mutations have differential effects both on ligand binding and ligand-induced Notch3 receptor signaling through RBP-Jk. Exp. Cell Res. *299*, 454–464.

Phng, L.K., and Gerhardt, H. (2009). Angiogenesis: a team effort coordinated by notch. Dev. Cell *16*, 196–208.

Ribatti, D., Nico, B., and Crivellato, E. (2011). The role of pericytes in angiogenesis. Int. J. Dev. Biol. *55*, 261–268.

Rustenhoven, J., Aalderink, M., Scotter, E.L., Oldfield, R.L., Bergin, P.S., Mee, E.W., Graham, E.S., Faull, R.L., Curtis, M.A., Park, T.I., et al. (2016). TGF-beta1 regulates human brain pericyte inflammatory processes involved in neurovasculature function. J. Neuroinflammation *13*, 37.

Sharma, P., Wang, T., Brown, M.J., and Schapira, A.H. (2001). Fits and strokes. Lancet *358*, 120.

Smyth, L.C.D., Rustenhoven, J., Scotter, E.L., Schweder, P., Faull, R.L.M., Park, T.I.H., and Dragunow, M. (2018). Markers for human brain pericytes and smooth muscle cells. J. Chem. Neuroanat. *92*, 48–60.

Stebbins, M.J., Gastfriend, B.D., Canfield, S.G., Lee, M.S., Richards, D., Faubion, M.G., Li, W.J., Daneman, R., Palecek, S.P., and Shusta, E.V. (2019). Human pluripotent stem cell-derived brain pericyte-like cells induce blood-brain barrier properties. Sci. Adv. *5*, eaau7375.

Stenborg, A., Kalimo, H., Viitanen, M., Terent, A., and Lind, L. (2007). Impaired endothelial function of forearm resistance arteries in CADASIL patients. Stroke *38*, 2692–2697.

Sweeney, M.D., Ayyadurai, S., and Zlokovic, B.V. (2016). Pericytes of the neurovascular unit: key functions and signaling pathways. Nat. Neurosci. *19*, 771–783.

Takahashi, K., and Yamanaka, S. (2006). Induction of pluripotent stem cells from mouse embryonic and adult fibroblast cultures by defined factors. Cell *126*, 663–676.

Tigges, U., Welser-Alves, J.V., Boroujerdi, A., and Milner, R. (2012). A novel and simple method for culturing pericytes from mouse brain. Microvasc. Res. *84*, 74–80.

Tiscornia, G., Vivas, E.L., and Izpisua Belmonte, J.C. (2011). Diseases in a dish: modeling human genetic disorders using induced pluripotent cells. Nat. Med. *17*, 1570–1576.

van Dijk, C.G., Nieuweboer, F.E., Pei, J.Y., Xu, Y.J., Burgisser, P., van Mulligen, E., el Azzouzi, H., Duncker, D.J., Verhaar, M.C., and Cheng, C. (2015). The complex mural cell: pericyte function in health and disease. Int. J. Cardiol. *190*, 75–89.

Vanlandewijck, M., He, L., Mae, M.A., Andrae, J., Ando, K., Del Gaudio, F., Nahar, K., Lebouvier, T., Laviña, B., Gouveia, L., et al. (2018). A molecular atlas of cell types and zonation in the brain vasculature. Nature *554*, 475–480.

Wallays, G., Nuyens, D., Silasi-Mansat, R., Souffreau, J., Callaerts-Vegh, Z., Van Nuffelen, A., Moons, L., D'Hooge, R., Lupu, F., Carmeliet, P., et al. (2011). Notch3 Arg170Cys knock-in mice display pathologic and clinical features of the neurovascular disorder cerebral autosomal dominant arteriopathy with subcortical infarcts and leukoencephalopathy. Arterioscler. Thromb. Vasc. Biol. *31*, 2881–2888.

Wang, T., Holt, C.M., Xu, C., Ridley, C., P O Jones, R., Baron, M., and Trump, D. (2007). Notch3 activation modulates cell growth behaviour and cross-talk to Wnt/TCF signalling pathway. Cell Signal. *19*, 2458–2467.

Wang, T., Baron, M., and Trump, D. (2008). An overview of Notch3 function in vascular smooth muscle cells. Prog. Biophys. Mol. Biol. *96*, 499–509.

Wang, Q., Zhao, N., Kennard, S., and Lilly, B. (2012). Notch2 and Notch3 function together to regulate vascular smooth muscle development. PLoS One *7*, e37365.

Wang, Y., Pan, L., Moens, C.B., and Appel, B. (2014). Notch3 establishes brain vascular integrity by regulating pericyte number. Development *141*, 307–317.

Winkler, E.A., Bell, R.D., and Zlokovic, B.V. (2011). Central nervous system pericytes in health and disease. Nat. Neurosci. *14*, 1398–1405.

Yao, Y., Chen, Z.L., Norris, E.H., and Strickland, S. (2014). Astrocytic laminin regulates pericyte differentiation and maintains blood brain barrier integrity. Nat. Commun. *5*, 3413.

Zechariah, A., ElAli, A., Doeppner, T.R., Jin, F., Hasan, M.R., Helfrich, I., Mies, G., and Hermann, D.M. (2013). Vascular endothelial growth factor promotes pericyte coverage of brain capillaries, improves cerebral blood flow during subsequent focal cerebral ischemia, and preserves the metabolic penumbra. Stroke *44*, 1690–1697.